

## RESEARCH ARTICLE

10.1002/2015JD024246

## Special Section:

East Asian Study of  
Tropospheric Aerosols and  
Impact on Cloud and  
Precipitation

## Key Points:

- Probabilities of precipitation differ considerably for different types of clouds found in China
- Rainfall amounts vary with AOD with a tipping point at a moderate AOD value
- Both aerosol-radiation interaction and aerosol-cloud interaction are found to impact cloud and precipitation

## Correspondence to:

Z. Li,  
zli@atmos.umd.edu

## Citation:

Jiang, M., Z. Li, B. Wan, and M. Cribb (2016), Impact of aerosols on precipitation from deep convective clouds in eastern China, *J. Geophys. Res. Atmos.*, 121, doi:10.1002/2015JD024246.

Received 19 SEP 2015

Accepted 1 JUL 2016

Accepted article online 7 JUL 2016

## Impact of aerosols on precipitation from deep convective clouds in eastern China

Mengjiao Jiang<sup>1,2</sup>, Zhanqing Li<sup>1,2</sup>, Bingcheng Wan<sup>3</sup>, and Maureen Cribb<sup>2</sup>

<sup>1</sup>State Key Laboratory of Earth Surface Processes and Resource Ecology, College of Global Change and Earth System Science, Beijing Normal University, Beijing, China, <sup>2</sup>Department of Atmospheric and Oceanic Science and ESSIC, University of Maryland, College Park, Maryland, USA, <sup>3</sup>State Key Laboratory of Atmospheric Boundary Layer Physics and Atmospheric Chemistry, Institute of Atmospheric Physics, Chinese Academy of Sciences, Beijing, China

**Abstract** We analyzed the impact of aerosols on precipitation based on 3 years of 3-hourly observations made in heavily polluted eastern China. The probability of precipitation from different cloud types was calculated using International Satellite Cloud Climatology Project cloud data and gauge-based hourly precipitation data. Because deep convective clouds have the largest precipitation probability, the influence of aerosols on the precipitation from such clouds was studied in particular. Aerosol properties were taken from the Modern-Era Retrospective Analysis for Research and Applications Aerosol Reanalysis data set. As aerosol optical depth increased, rainfall amounts from deep convective clouds increased at first and then decreased. The descending part of the trend is likely due to the aerosol radiative effect. Downwelling solar radiative fluxes at the surface decreased as aerosol optical depth increased. The decrease in solar radiation led to a decrease in ground heat fluxes and convective available potential energy, which is unfavorable for development of convective clouds and precipitation. The tendencies for lower cloud top temperatures, lower cloud top pressures, and higher cloud optical depths as a response to larger aerosol optical depths suggest the invigoration effect. Vertical velocity, relative humidity, and air temperature from the National Centers for Environmental Prediction Climate Forecast System Reanalysis were sorted to help investigate if the trends are dependent on any environmental conditions. How dynamic and microphysical factors strengthen or mitigate the impact of aerosols on clouds and precipitation and more details about their interplay should be studied further using more observations and model simulations.

## 1. Introduction

The effects of aerosols on clouds and precipitation are complex and important and have motivated an increasing number of studies [Twomey *et al.*, 1984; Albrecht, 1989; Kaufman and Fraser, 1997; Rosenfeld, 1999; Ackerman *et al.*, 2000]. A variety of data sets have been employed, as reviewed by Tao *et al.* [2012]. They include data from satellite platforms [Rosenfeld and Lensky, 1998; Rosenfeld, 2000; Koren *et al.*, 2005; Lin *et al.*, 2006; Yuan *et al.*, 2008; Niu and Li, 2012; Peng *et al.*, 2016], ground-based observations [Feingold, 2003; Andreae *et al.*, 2004; Li *et al.*, 2011a], and model simulations [Wang, 2005; Jiang *et al.*, 2006; Cheng *et al.*, 2007; van den Heever and Cotton, 2007; Li *et al.*, 2008; Fan *et al.*, 2009; Wang *et al.*, 2011; Fan *et al.*, 2015]. Each approach has its merits and limitations in identifying and understanding the effects of aerosols on clouds and precipitation. While a wide variety of aerosol effects under different constraints and conditions have been reported, the most important effects originate from the aerosol-radiation interaction (ARI) and the aerosol-cloud interaction (ACI), which are new terms coined by the most recent Intergovernmental Panel on Climate Change [Intergovernmental Panel on Climate Change, 2013]. They describe how aerosols affect the scattering and absorption of radiation and cloud properties, respectively. This has expanded the research field to include the study of dynamic and thermodynamic responses of these aerosol-induced perturbations and the interactions between them.

Water vapor transport, the vertical motion of air, and cloud microphysics are three important factors that determine deep convective cloud and precipitation amount. Aerosols affect these three factors through ARI and ACI processes. In the ARI process, a higher aerosol loading can lead to a reduction in solar radiation reaching the ground due to both aerosol scattering and absorption and an increase in atmospheric absorption of solar radiation by absorbing aerosols [Rosenfeld *et al.*, 2008; Li *et al.*, 2010]. As a consequence, ground fluxes (sensible and latent heat), precipitation, and other meteorological variables are affected [Ackerman, 1977; Barbaro *et al.*, 2014; Grant and van den Heever, 2014]. Aerosol effects on atmospheric stability, and consequently precipitation, have a significant impact in heavily polluted regions [Ackerman, 1977]. Also, sensible

and latent fluxes will respond differently to the presence of aerosols depending on soil properties like soil moisture [Grant and van den Heever, 2014]. The aerosol vertical distribution within the atmospheric boundary layer also affects its dynamics and may play a role in cloud formation. By combining observations and model simulations, Barbaro *et al.* [2014] found that absorbing aerosols help increase the heating rate in the atmosphere, which leads to a higher afternoon convective boundary layer height, while scattering aerosols contribute to smaller heating rates and to a shallower convective boundary layer height. The sensitivity of convective boundary layer dynamics and ground fluxes to aerosol loading highlights the need for considering aerosol radiative perturbations in the aerosol-cloud-land surface system.

In the ACI process, the main role of aerosols is to act as cloud condensation nuclei (CCN) and ice nuclei in the formation and development of clouds. The aerosol invigoration effect (AIV) hypothesis [Rosenfeld *et al.*, 2008] for deep convective clouds refers to the fact that more CCN leads to delays in precipitation formation due to collision-coalescence, which allows for more condensation and freezing, and ultimately to the release of extra latent heat to fuel convection. The AIV phenomenon is consistent with observational findings [Andreae *et al.*, 2004; Li *et al.*, 2011a]. Koren *et al.* [2014] also identified the AIV for warm clouds from observations and numerical model simulations. Fan *et al.* [2009] concluded that the AIV favors weak shear in warm-based convection. The AIV is not limited to increasing cloud thickness but can also affect the horizontal extent of clouds, especially the anvil size [Koren *et al.*, 2010; Yan *et al.*, 2014], which can be explained by the aerosol microphysical, or Twomey, effect [Fan *et al.*, 2013]. However, whether the increase in buoyancy due to more condensation and extra latent heat release is large enough to compensate for the decrease caused by the drag associated with condensate loading is still in question. Some studies have shown that there is an optimal value of aerosol loading in invigoration [Rosenfeld *et al.*, 2008; Koren *et al.*, 2008], while others have shown that changes in latent heating were, on average, an order of magnitude smaller than those in the condensate loading term [Storer and van den Heever, 2013; Lebo, 2014]. Other studies have pointed to other pathways involved with the ACI, such as the cold pool effect [Tao *et al.*, 2007; Lebo and Morrison, 2014; Lebo, 2014; Grant and van den Heever, 2015]. Aerosols affect the cold pool through changes in evaporation due to perturbations in raindrop size and number. The impact of aerosols on the behavior of the cold pool is modulated by different configurations of low-level wind shear [Tao *et al.*, 2007; Lebo and Morrison, 2014] or the midlevel dry layer [Grant and van den Heever, 2015].

Note that the ARI and the ACI do not exist in isolation but rather interact with each other. In addition, aerosol-induced effects also interact with environmental dynamic, heat, and water vapor conditions. Fan *et al.* [2015] showed that aerosol-enhanced conditional instability in the Sichuan Basin suppresses convection and precipitation in the basin. As the accumulated water vapor is transported to the downstream mountain area by atmospheric circulation, the excess water vapor is lifted by the topography and causes catastrophic flooding. The combination of and competition between ARI and ACI effects of aerosols has been hypothesized and supported by observational data to some degree [Rosenfeld *et al.*, 2008; Koren *et al.*, 2008; Wu *et al.*, 2016; Guo *et al.*, 2016].

The objective of this study is to examine both effects in dictating precipitation by analyzing a large ensemble of observational data sets. To this end, we choose eastern China as the study region because convective activity often occurs there and aerosol loading is exceptionally high [Xin *et al.*, 2007; Lee *et al.*, 2010; Li *et al.*, 2007, 2011b]. Several data sets are employed including satellite retrievals, ground-based measurements, and reanalysis data. These data sets are described in section 2, followed by a description of the methodology. Through sorting rainfall data into different aerosol optical depth (AOD) bins, comparisons of rainfall amount for varying levels of polluted conditions are made. The changes in downwelling surface shortwave radiation, ground heat fluxes, and convective available potential energy (CAPE) with AOD are analyzed. Vertical velocity (VV) at 500 mb, 2 m level relative humidity (RH), and 2 m level air temperature (AT) from the National Centers for Environmental Prediction (NCEP) Climate Forecast System Reanalysis (CFSR) are sorted to investigate whether the detected trends are dependent on environmental conditions. The bootstrap confidence interval test is conducted to analyze the statistical significance of the trends. Results are presented in section 3, followed by a summary and discussion in section 4.

## 2. Data, Methodology, and the Research Domain

### 2.1. Data

Four data sets from the year 2005 to 2007 are used in this study: (1) clouds: the International Satellite Cloud Climatology Project (ISCCP) product to take advantage of its relatively high temporal sampling rate relative to

**Table 1.** Variables From the ISCCP Product Used in the Study<sup>a</sup>

Variables (Units)	Availability
IR-retrieved cloud top temperature (K)	daytime, nighttime
IR-retrieved cloud top pressure (hPa)	daytime, nighttime
VIS-retrieved liquid cloud tau (unitless)	daytime
VIS-retrieved ice cloud tau (unitless)	daytime

<sup>a</sup>IR: infrared; VIS: visible.

Sun-synchronous satellite products, (2) precipitation: the gauge-based hourly analyses generated by the China Meteorological Administration (CMA) National Meteorological Information Center (NMIC), (3) aerosols: the Modern-Era Retrospective Analysis for Research and Applications (MERRA) aerosol reanalysis, and (4) atmospheric parameters: the NCEP CFSR.

### 2.1.1. ISCCP Cloud Data

The ISCCP was established in 1982 as part of the World Climate Research Program and data collection began on 1 July 1983 (<http://isccp.giss.nasa.gov/overview.html>). The first global-scale maps of the spatial distribution of clouds and their properties were generated from the research effort [Schiffer and Rossow, 1983]. Many studies have been done to validate the ISCCP product on a global scale [Rossow and Garder, 1993; Rossow et al., 1993; Hahn et al., 2001] and over certain regions of the world such as China [Wei et al., 1996; Weng and Han, 1998]. The D-series version of cloud products [Rossow and Schiffer, 1999] is used in this study. The products used are the cloud top temperature (CTT) and pressure (CTP) and liquid and ice cloud optical depth (COD) (see Table 1). The horizontal resolution of the pixel-level data is about 30 km, and the products are generated at 3-hourly intervals thanks to the use of geostationary satellite data. The threshold value of CTT used to distinguish between liquid and ice clouds is 260 K. Only daytime data are used because of the use of the visible channel in the ISCCP data set to calculate COD. Data from 2005 to 2007 are used in this study.

### 2.1.2. Gauge-Based Analysis of Hourly Precipitation Over China

Ground-based observations of precipitation are regarded as “truth” when evaluating satellite observations and model results. Precipitation data collected at short timescales (<24 h) are needed because the duration of most precipitation events ranges from minutes to hours. Measurements on these timescales are not only rare but also restricted to limited times in many regions. Hence, hourly gauge-based precipitation analyses with high spatial and temporal resolutions are of great value, especially in China.

The precipitation data used in this study are taken from the gauge-based hourly analyses [Shen et al., 2010] generated by the NMIC of the CMA. The database is composed of hourly precipitation reports from ~2000 automatic weather stations located across China. The following data quality checks are first made by staff at the CMA/NMIC: (1) a check for extreme values, where if the value exceeds the monthly maximum in daily precipitation, the value is rejected; (2) an internal consistency check to identify erroneous reports caused by incorrect units, reading, or coding; and (3) a spatial consistency check where the time series of hourly precipitation at a particular station and that from nearby stations are compared [Shen et al., 2010]. Data are rejected if they fail any of these checks. A  $0.25^\circ \times 0.25^\circ$  gridded analyzed field over China is then constructed based on station data using the objective analysis technique described by Xie et al. [2007]. Interim gridded fields of the ratio of hourly precipitation to the daily climatology are obtained using the optimal interpolation method [Gandin, 1965]. The final  $0.25^\circ$  latitude/longitude gridded hourly precipitation field is calculated by multiplying the daily climatology by the hourly ratio. After all these steps are performed, a gauge-based hourly gridded precipitation data set is constructed [Shen et al., 2010]. The automatic weather stations in eastern China are evenly distributed [Shen et al., 2010]. This data set covers the period of 2005 to 2007.

### 2.1.3. MERRA Aerosol Reanalysis (MERRAero)

The latest MERRA reanalysis was undertaken by NASA for the satellite era (1979 to present) using version 5 of the Goddard Earth Observing System Data Assimilation System (GEOS-5) [Rienecker et al., 2011]. The GEOS-5 not only contains atmospheric components, ocean circulation and biogeochemistry, and land surface processes, but also includes modules representing aerosols and tropospheric/stratospheric chemical constituents [Rienecker et al., 2011] (<http://gmao.gsfc.nasa.gov/MERRA/>).

The aerosol module is largely based on the Goddard Chemistry, Aerosol, Radiation, and Transport (GOCART) model [Chin et al., 2002]. The GOCART model incorporates aerosol and precursor emissions from fossil fuel/biofuel combustions, biomass burning, and natural sources (volcanoes, deserts, and oceans) and is driven by the reanalysis meteorological fields to simulate aerosol distributions and tendencies [Chin et al., 2013]. For this reason, the MERRAero has five aerosol species, namely, dust, sea salt, sulfates, organic carbon,

**Table 2.** Variables From the CFSR Product Used in the Study

Variables	Unit	Temporal Resolution	Spatial Resolution
Convective available potential energy	$\text{J kg}^{-1}$	3-hourly	$0.5^\circ \times 0.5^\circ$
Vertical velocity	$\text{Pa s}^{-1}$	3-hourly	$0.5^\circ \times 0.5^\circ$
Relative humidity	%	3-hourly	$0.5^\circ \times 0.5^\circ$
2 m temperature	K	3-hourly	$0.312^\circ \times 0.312^\circ$
Sensible heat flux	$\text{W m}^{-2}$	3-hourly	$0.312^\circ \times 0.312^\circ$
Latent heat flux	$\text{W m}^{-2}$	3-hourly	$0.312^\circ \times 0.312^\circ$
Downward shortwave radiation	$\text{W m}^{-2}$	3-hourly	$0.312^\circ \times 0.312^\circ$

and black carbon. Both dry deposition and wet deposition are considered in the model setting [Chin et al., 2002]. Details about the different emissions and configurations are described by Buchard et al. [2015].

For this MERRAero reanalysis, GEOS-5 runs at a nominal 50 km horizontal resolution with 72 vertical layers (top of the atmosphere at ~85 km) and is constrained by MERRA meteorology [da Silva et al., 2011]. The data assimilation system is the Grid-point Statistical Interpolation developed by the NCEP [Rienecker et al., 2008]. The bias-corrected AOD from Moderate Resolution Imaging Spectroradiometer (MODIS) observations is included in the AOD assimilation. The correction is made by integrating MODIS radiances with Aerosol Robotic Network-calibrated AOD using a neural network method with careful cloud screening. Quality control is done using an adaptive buddy check scheme [Dee et al., 2001]. The spatial resolution of the data is  $0.625^\circ \times 0.5^\circ$  longitude by latitude, and the data length is from 2002 to the present. The evaluation and analyses of MERRAero data have been done using different satellite retrievals and observations [Kishcha et al., 2014; Buchard et al., 2015; Nowottnick et al., 2015]. Hourly total AOD at 550 nm data for the years 2005 to 2007 are used in this study.

#### 2.1.4. The NCEP CFSR

The CFSR is an advanced high-resolution, coupled atmosphere-ocean-land surface-sea ice system that includes an interactive sea ice model and the assimilation of satellite radiances (<http://rda.ucar.edu/pub/cfsr.html>). The NCEP CFSR covers the 31 year period from 1979 to 2009. Representing the new generation of reanalysis, the CFSR has advantages in both time and space resolutions. The consideration of observed variations in carbon dioxide and other changes in aerosols and other trace gases, solar variations in the atmospheric model over 31 years, and direct use of satellite observed radiances helps to better provide detailed estimates of the Earth system [Saha et al., 2010]. A subset of the data set called “NCEP CFSR Selected Hourly Time-Series Products, January 1979 to December 2010” is used in this study. Data from 1 January 2005 to 31 December 2007 were obtained from the Computational Information Systems Laboratory Research Data Archive (<http://rda.ucar.edu/datasets/ds093.1/>), which provides the best estimate of the state of these coupled research domains during the study period of interest here. Downward shortwave radiation, sensible/latent heat fluxes, CAPE, 500 mb VV, 2 m RH, and 2 m AT was extracted from CFSR data sets and is summarized in Table 2. The latitude-longitude spatial resolution of the data is greater than  $0.5^\circ \times 0.5^\circ$ . More details about the CFSR are described by Saha et al. [2010].

#### 2.2. Methodology

All data in this study are processed at a temporal resolution of 3 h. The probability of different levels of precipitation from different cloud types is calculated using ISCCP cloud data and gauge-based precipitation data, based on the classification of ISCCP cloud types and the classification of gauge-based hourly rainfall. Different levels of rainfall from deep convective clouds are examined under different AOD conditions using MERRAero AOD data. To analyze the correlation between rainfall and aerosols, downward shortwave radiation reaching

the surface, ground heat fluxes, CAPE, and cloud properties are examined under changing AOD conditions. To highlight the response of precipitation and CAPE to aerosols under different environmental conditions, VV, RH, and AT are divided into high and low groups, and trends in each group are examined separately.

**Table 3.** Definitions of Rain Levels Used in the Study

Rain Level	Rain Amount ( $\text{mm h}^{-1}$ )
Light rain	0–2.5
Moderate rain	2.6–8.0
Heavy rain	8.1–15.9
Rainstorm	$\geq 16.0$

**Table 4.** Probability of Precipitation From Different Clouds Over China

Cloud Type	Light Rain	Moderate Rain	Heavy Rain	Rainstorm	Total
Deep convection	33.60%	3.69%	0.45%	0.07%	37.80%
Nimbostratus	33.20%	1.87%	0.15%	0.02%	35.23%
Stratus	27.11%	1.50%	0.12%	0.01%	28.74%
Cirrostratus	20.38%	1.66%	0.21%	0.04%	22.28%
Altostratus	16.47%	0.89%	0.09%	0.01%	17.47%
Stratocumulus	9.97%	0.58%	0.06%	0.01%	10.62%
Cirrus	10.44%	0.72%	0.09%	0.02%	11.26%
Alto cumulus	7.28%	0.32%	0.04%	0.01%	7.65%
Cumulus	4.62%	0.22%	0.02%	0.00%	4.87%

### 2.2.1. Cloud and Rainfall Classification

Clouds are classified according to the ISCCP cloud classification scheme [Rossow and Schiffer, 1999]. The scheme uses CTP and COD to classify clouds into nine types: COD: 0–3.6, cumulus (low level), alto cumulus (middle level), cirrus (high level); COD: 3.6–23, stratocumulus (low level), altostratus (middle level), cirrostratus (high level); COD: 23–379, stratus (low level), nimbostratus (middle level), and deep convection (high level). The CTP for low, middle, and high level is 680–1000, 440–680, and 50–440, respectively.

Hourly rain level criteria from the Office of China Flood Prevention and Drought Resistance Headquarters' flood prevention manual are used to classify rain levels [Zhang and Li, 1992]. Four levels of rain are identified (Table 3): light rain (less than 2.5 mm h<sup>-1</sup>), moderate rain (2.6–8.0 mm h<sup>-1</sup>), heavy rain (8.1–15.9 mm h<sup>-1</sup>), and rainstorm (greater than 16.0 mm h<sup>-1</sup>).

### 2.2.2. Calculation of the Probability of Precipitation

The probability of precipitation is based upon tallies from the 36 rainfall level/cloud-type combinations. The probability of rain level *i*, occurring from cloud type *j*,  $P_{rij}$ , is calculated as

$$P_{rij} = N_{rij}/N_j, \quad (1)$$

$$i = 1, 4; j = 1, 9$$

where  $N_{rij}$  is the tally of cases where rain level *i* occurs from cloud type *j* and  $N_j$  is the total number of cases where the cloud is cloud type *j*.

### 2.2.3. Choice of Cloud Type

Precipitation is largely associated with cloud type. We calculated the probability of different levels of precipitation from different cloud types over China using the method described in section 2.2.2. Results are summarized in Tables 4 and 5 (June–July–August only). The probability of precipitation from deep convective clouds is 37.80%, which is almost 8 times greater than that for cumulus clouds (4.87%) and is higher in summer (42.46%). Because deep convective clouds are driven by strong convection which fuels ACIs [Tao et al., 2012], this cloud type is also a major focus of ACI studies. Deep convective clouds are thus chosen to study the impact of aerosols on precipitation here, which is also a major frontier in aerosol-cloud-precipitation studies.

### 2.2.4. Choice of Research Domain

Figure 1a shows the research domain. The domain covers the area east of 100°E, south of 40°N and bordered by the eastern coastline. This region is chosen because (1) AODs are relatively higher here (Figure 1b) and (2) the frequency of deep convection (Figure 1c) and the probability of precipitation from deep convection (Figure 1d) appear greater here than in other parts of China.

**Table 5.** Same as Table 4 but for June, July, and August Only

Cloud Type	Light Rain	Moderate Rain	Heavy Rain	Rainstorm	Total
Deep convection	36.72%	4.95%	0.67%	0.11%	42.46%
Nimbostratus	33.37%	3.04%	0.31%	0.03%	36.75%
Stratus	25.42%	2.72%	0.27%	0.03%	28.45%
Cirrostratus	26.37%	2.50%	0.33%	0.05%	29.26%
Altostratus	21.00%	1.42%	0.15%	0.02%	22.58%
Stratocumulus	12.71%	0.96%	0.11%	0.01%	13.80%
Cirrus	17.86%	1.58%	0.21%	0.03%	19.68%
Alto cumulus	12.77%	0.75%	0.07%	0.01%	13.60%
Cumulus	7.35%	0.48%	0.05%	0.00%	7.88%

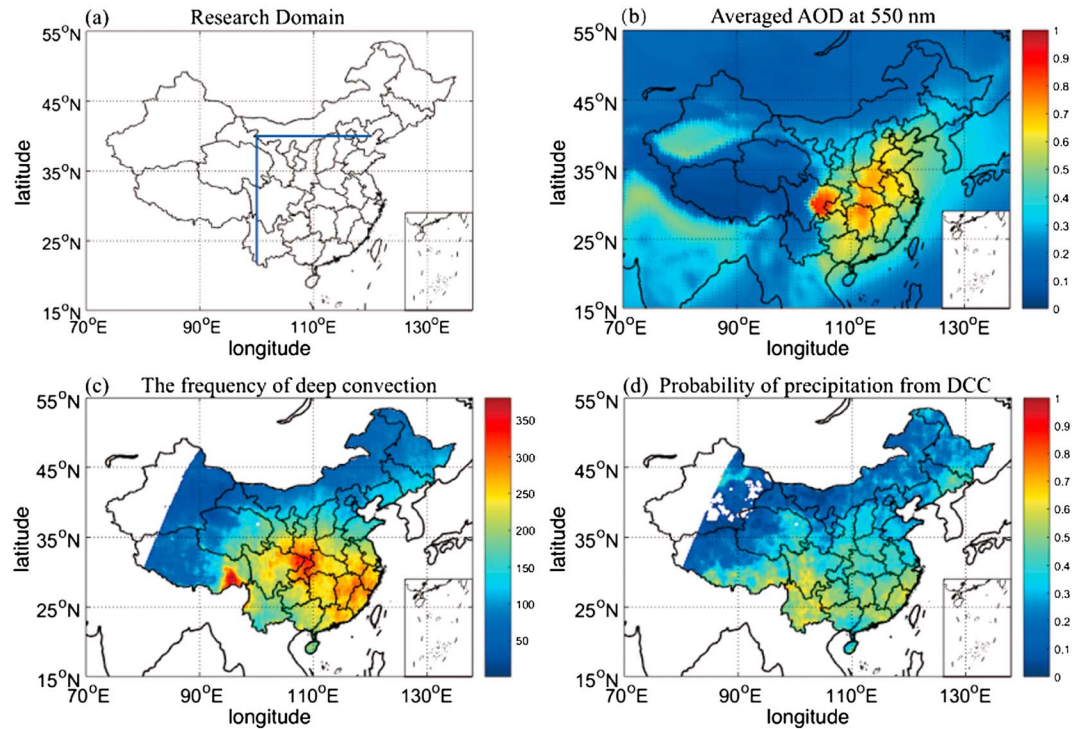


**Figure 1.** (a) Map of China with the topmost and western boundary of the study area outlined in blue. The land-only study area stretches eastward from 100°E to the seas and southward from 40°N to the South China Sea. (b) Spatial distribution of annually averaged total AOD over China from the MERRAero AOD reanalysis. (c) The number of deep convective cloud occurrences over China. (d) Probability of precipitation from deep convective clouds over China. Data are from 2005 to 2007.

### 2.2.5. Spatial and Temporal Matching of Data and Choice of Study Cases

MERRAero AOD data are averaged over the 3 h before the time when a deep convective cloud is identified. For example, say that a cloud at 0300 coordinated universal time (UT) is identified as a deep convective cloud in the ISCCP data set. We assume that aerosols' main role in the formation of this cloud occurred from 0000 to 0300 UT and average AOD conditions during this period are used. Precipitation from 0300–0400, 0400–0500, and 0500–0600 UT is summed and used to represent precipitation from that at 0300 UT deep convective cloud. Variables from the CFSR are compiled at the time the deep convective cloud was identified and before the onset of precipitation, which in this example is at 0300 UT. When a deep convective cloud was identified, we further checked if precipitation occurred during the 3 h after the time when the cloud was identified. If precipitation occurred, cases with no precipitation during the 3 h time interval before the time when the cloud was identified are retained to minimize the influence of prior rainfall on AOD through the wet deposition process.

The horizontal resolution of ISCCP pixel-level data is approximately 30 km, which is very close to the resolution of the precipitation data. The “cubic” interpolation technique was used to interpolate ISCCP pixel-level data to the same grid as the gauge-based precipitation field. MERRAero AOD data and CFSR data were regridded to the same grids as those used for clouds and precipitation using the “nearest-neighbor” interpolation technique.

The spatial and temporal resolutions of the matched data sets are  $0.25^\circ \times 0.25^\circ$  and 3-hourly averages. There are ~139,000 chosen grid points in total. Four AOD bins are selected to further check if there is any corresponding change in cloud properties, radiative properties, CAPE, and precipitation to variations in AOD. The AOD bins are  $<0.25$ ,  $0.25\text{--}0.50$ ,  $0.50\text{--}0.75$ , and  $>0.75$ . The proportion of data points in each bin is 20%, 28%, 22%, and 30%, respectively. Note that uncertainties are incurred in the use of these matched data. The motion of air mass is omitted because the variation in aerosols is much smaller than that of clouds [Gryspeerdt et al., 2014a]. Even though the air mass could be advected through three grid points

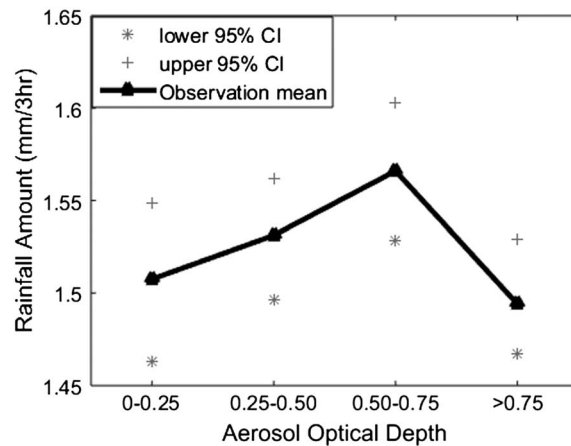


**Figure 2.** Rainfall amount from deep convective clouds as a function of aerosol optical depth. The solid line shows the mean trend from 3 years of observations. The plus and asterisk marks show the bootstrap confidence interval of the mean at the 95% confidence interval.

is constructed. The bootstrap distribution gives information about the sampling distribution. Bootstrap method is a nonparametric method. The interval between the 2.5% and 97.5% percentiles of the bootstrap distribution of the mean defines the bootstrap percentile confidence interval for the corresponding parameter at a 95% confidence level.

The segmented trend test is used in the study. The steps followed to test the significance of the trends are as follows:

1. Set the null hypothesis,  $H_0$ : there is no difference in the true means of the observations in the two AOD bin groups, i.e.,  $H_0: \mu_1 = \mu_2$ , where  $\mu_1$  and  $\mu_2$  are the population means for the first group (with a larger mean value) and the second group (with a smaller mean value), respectively. The one-sided alternative hypothesis is  $\mu_1 > \mu_2$ .
2. Draw a resample of size  $n$  with replacement from the first group and a resample of size  $m$  with replacement from the second group then compute the difference between the two sample means from the two groups.
3. Repeat this resampling process 1000 times.
4. Construct the bootstrap distribution of the statistic and do the bootstrap confidence intervals test. If the confidence interval fails to include the null hypothesis value, then we reject  $H_0$  at the corresponding significance level.

The test  $P$  value is set as 0.05 in this study.

### 3. Results

#### 3.1. Observations of Changes in Rainfall Amounts With AOD

Rainfall amounts from deep convective clouds as a function of AOD are shown in Figure 2. The solid line shows the mean trend from 3 years of observations, and the asterisks and plus marks indicate lower and upper 95% confidence intervals of the bootstrap mean, respectively. The standard deviations of mean rainfall amount in each AOD bin are 0.0200, 0.0173, 0.02, and 0.0156, respectively. Precipitation from deep convective clouds increases as AOD increases from low to moderate values then decreases as AOD increases from moderate to high values. The  $P$  value is 0.024 for the increasing trend and 0.003 for the decreasing trend, which are less than 0.05. The null hypothesis that there is no aerosol effect on rainfall amount is rejected at the corresponding significance level. The up-and-down trend of rainfall amount with AOD is statistically significant. To better compare the rainfall amounts, we classified all data according to the four rain level categories. Figure 3 shows rainfall amount as a function of AOD in each rainfall amount category. The up-and-down trend is seen for moderate rain and rainstorm categories. For light rain and heavy rain

during those 3 h, the AOD would not change much. Multilayer cloud cases are not considered here because their interactions with aerosols are more complex. We also acknowledge some shortcomings of the ISCCP satellite product, namely, in detecting multilayer clouds and in the cloud classification method.

#### 2.2.6. Statistical Analysis

The bootstrap percentile method described by Hesterberg *et al.* [2006] is used to represent the spread about the mean in each AOD bin. The key point of the bootstrap method is that it creates many resamples by sampling with “replacement” from the original samples. The word replacement means that in this method, we draw an observation from the original sample and then put it back before drawing another observation. This resampling is repeated many times (usually more than 1000 times), and then a bootstrap distribution

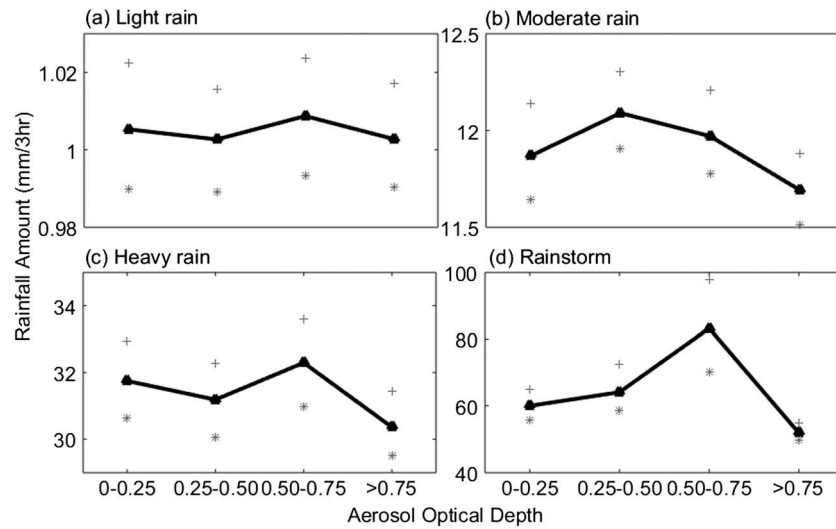


**Figure 3.** Mean rainfall amount from deep convective clouds as a function of aerosol optical depth range for (a) light rain, (b) moderate rain, (c) heavy rain, and (d) rainstorm categories. The solid line shows the mean trends from 3 years of observations. The plus and asterisk marks show the bootstrap confidence interval of the mean at the 95% confidence interval.

categories, there is no such trend. For moderate rain (Figure 3b), the turning point is located in the 0.25–0.50 AOD bin. The decreasing trend is statistically significant with a *P* value of 0.005, while the increasing trend is not (*P* value equal to 0.092). For the rainstorm category (Figure 3d), the average rainfall amount in each

AOD bin is 60, 64.11, 83.26, and 55.59 mm, respectively. The standard deviations of the mean rainfall amount in each bin are 2.46488, 3.6671, 6.8704, and 1.2859, respectively. The aerosol perturbation to deep convective rainfall amounts is not monotonic. In the following sections, the ACI and the ARI are considered as potential contributors to this up-and-down trend in rainfall amounts from deep convective clouds as AOD increases.

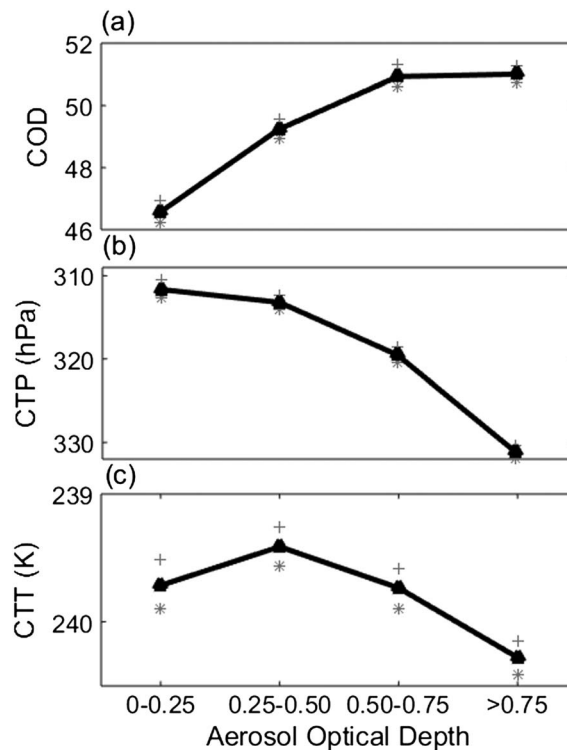


**Figure 4.** (a) Cloud optical depth, (b) cloud top pressure, and (c) cloud top temperature as a function of aerosol optical depth range. The solid line shows the mean trends from 3 years of observations. The plus and asterisk marks show the bootstrap confidence interval of the mean at the 95% confidence interval.

### 3.2. The Response of Cloud Properties to AOD

The COD, CTP, and CTT as a function of AOD are shown in Figure 4. The mean COD (Figure 4a) increases from 46.57 in the 0–0.25 AOD bin to 49.59 in the 0.25–0.50 AOD bin and to 50.93 in the 0.50–0.75 AOD bin then decreases to 50.73 in the >0.75 AOD bin. While the increasing trend is significant, the decreasing trend is not. Note that the directions of the *Y* ordinates in Figures 4b and 4c are reversed. The CTP increases with AOD. The mean CTP in each AOD bin is 311.7, 313.2, 320.7, and 327.5 hPa, respectively. The decreasing, then increasing, trend in CTT is statistically significant. Lower CTP and CTT values suggest the development of clouds higher in the atmosphere. The responses of COD, CTP, and CTT to increasing AOD demonstrate the cloud invigoration

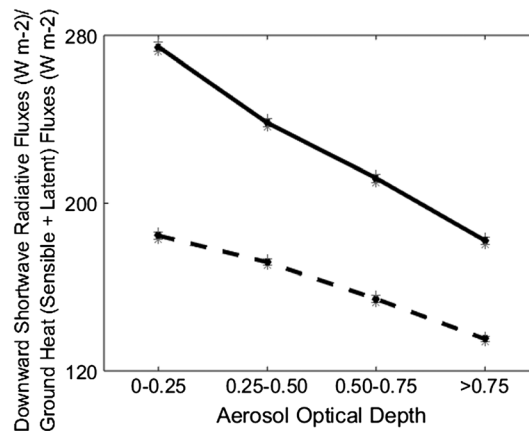


**Figure 5.** Mean downwelling solar radiation at the surface (solid line) and mean ground heat (sensible + latent) fluxes (dotted line) under deep convective cloudy sky conditions as a function of aerosol optical depth range. The solid and dotted lines show the mean trends from 3 years of observations. The plus and asterisk marks show the bootstrap confidence interval of the mean at the 95% confidence interval.

another pathway through which aerosols may affect precipitation [Tao et al., 2007; Lebo and Morrison, 2014; Lebo, 2014; Grant and van den Heever, 2015]. Specifically, the impact of aerosols on the behavior of the cold pool is modulated by the different settings of low-level wind shear [Tao et al., 2007; Lebo and Morrison, 2014] or the midlevel dry layer [Grant and van den Heever, 2015]. If stronger evaporative cooling is produced under high aerosol loading conditions, a stronger cold pool can be generated, which leads to low-level convergence through interactions with the low-level wind shear. For squall lines, if aerosols affect the cold pool to the point where an optimal balance between the cold pool and low-level wind shear-induced vorticities is reached, clouds are invigorated. If the midlevel dry layer is near the cloud base, this will lead to a stronger cold pool and subsequently, to greater precipitation totals. The mechanisms explaining this increasing branch of the trend are different, so it is difficult to pinpoint which one is at play from the analysis of the data sets alone.

### 3.3. The Response of Radiative and Thermal Properties to AOD

Aerosols perturb radiative and thermal properties by scattering and absorbing radiances. The impact of aerosols on precipitation may be related to the aerosol-induced changes in atmospheric heating and surface cooling. Downwelling shortwave radiative fluxes at the surface under deep convective cloudy sky conditions as a function of AOD are shown in Figure 5. Mean radiative fluxes in each AOD bin are 277.4, 235.6, 209.0, and 191.7  $\text{W m}^{-2}$ , respectively. A descending trend in mean ground heat fluxes as AOD increases is seen (Figure 5). Mean ground heat fluxes in each AOD bin are 184.5, 170, 152.4, and 141.9  $\text{W m}^{-2}$ , respectively. The boundaries of the confidence interval of observed means calculated at the 95% confidence level and marked by pluses and asterisks also decrease, indicating the statistical significance of these decreasing trends. The aerosol radiative effect usually reduces the amount of shortwave radiation reaching the surface, which leads to less sensible heat and latent heat transported from the surface to the atmosphere. Note that the radiative effect takes place directly under clear-sky conditions and indirectly under cloudy conditions by altering cloud properties and cloud radiative effects. In the >0.75 AOD bin, less radiation reaches the surface. If the reduction is mainly due to a larger cloud fraction, a higher COD is expected in the >0.75 AOD bin. However, there is a reduction in COD when going from the 0.50–0.75 AOD bin to the >0.75 AOD bin (Figure 4a). We thus infer that in addition to the impact of clouds on solar radiation, there also exists the impact of aerosols and aerosol-moderated cloud properties on radiative properties.

These processes can alter the moisture and thermal conditions of the atmosphere and the surface. CAPE is determined from the moisture and heating conditions in the atmosphere. Mean CAPE as a function of AOD is shown in Figure 6. Mean CAPE values and the 95% confidence level values of the bootstrap mean

phenomenon under specific AOD conditions. More importantly, the aerosol perturbation on deep convective clouds is not a monotonic function of AOD.

The AIV [Rosenfeld et al., 2008] likely explains the increasing part of the trend seen in the observations. Clouds occurring under higher aerosol loading conditions tend to suppress warm rain and to develop higher into the atmosphere. The freezing level is reached where additional latent heat is released to fuel cloud development. This phenomenon has been reported in numerous studies involving short-term aircraft data and long-term ground-based and spaceborne measurements [e.g., Andreae et al., 2004; Koren et al., 2005; Rosenfeld et al., 2008; Li et al., 2011a; Niu and Li, 2012; Peng et al., 2016]. The impact of aerosols on the cold pool through changes in evaporation due to the perturbation in raindrop size and number is

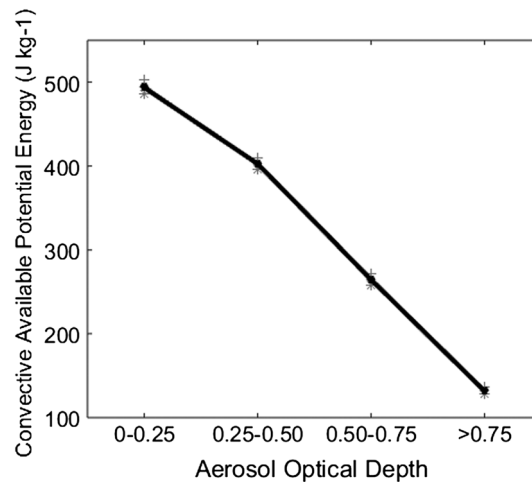


**Figure 6.** Mean convective available potential energy before the onset of precipitation as a function of aerosol optical depth range. The solid line shows the mean trends from 3 years of observations. The plus and asterisk marks show the bootstrap confidence interval of the mean at the 95% confidence interval.

decrease as AOD increases. In the  $>0.75$  AOD bin, the mean CAPE value is less than half of that in the 0–0.25 AOD bin. Mean CAPE values in each AOD bin are 494, 402.7, 257.3, and 177.2 J kg<sup>-1</sup>, respectively. Considering the important role of convection in the development of deep convective clouds that produce precipitation, the development of deep convective clouds and the precipitation associated with these clouds are highly influenced by CAPE [Rosenfeld *et al.*, 2008].

It should be mentioned that the increase in buoyancy due to the extra latent heat release by freezing is not included in the CFSR CAPE calculation (<http://www.emc.ncep.noaa.gov/mmb/papers/chuang/1/OF438.html>). Assuming that the invigoration effect exists in reality, invigoration and extra latent heating from freezing will result in more warming aloft in cloud. However, this is not considered in the CFSR data set, which uses the “original” CAPE calculation.

On the contrary, a reduction in CFSR CAPE is reached due to the environment aloft being warmer after the invigorated convection has dissipated. In addition, the decrease in CAPE can also be shown from the ARI perspective, i.e., a higher aerosol loading can lead to a reduction in solar radiation reaching the ground and to smaller magnitudes of ground fluxes. It is not easy to separate the different contributions to CAPE, especially CAPE values based on environmental profiles. Perhaps well-designed calculations can help, but certain assumptions must still be made. At least the changes in cloud properties suggest invigoration, although invigoration is difficult to prove from the quantification of aerosol-induced changes in CAPE.

### 3.4. Impact of Aerosols on Precipitation

The combined effects of aerosols on precipitation from deep convective clouds are complex and cannot be easily distinguished during the precipitation process. However, the similar up-and-down trends in cloud properties and rainfall amounts from deep convective clouds as AOD increases imply the potential influence of aerosols on precipitation. Owing to the joint influences of both the ARI and the ACI, or other aerosol perturbations on dynamic and thermodynamic factors, it has been hypothesized that the impact of aerosols on precipitation from deep convective clouds is not a monotonic function of AOD but peaks at a moderate level of AOD. Below this optimal AOD value, invigoration dominates, fueling the development of deep convective clouds with increasing AOD. Beyond that, invigoration yields to the ARI where CAPE is suppressed by increasing the AOD. Overall, it is the combination of these effects that affects precipitation via their influences on the profiles of both temperature and moisture, which determines convection in deep convective clouds and perturbations in cloud properties. The up-and-down trend of the response of cloud properties and rainfall found by Rosenfeld *et al.* [2008], Fan *et al.* [2009], and Koren *et al.* [2014] using model calculations, model simulations, or a combination of observations and model simulations appears to be consistent with our observational findings shown in Figures 2 and 4.

The various environmental effects on precipitation make it difficult to isolate the signal of aerosols [Wall *et al.*, 2014]. The effects of aerosols on precipitation and CAPE are influenced by cloud regimes and meteorological covariations [Gryspeerd *et al.*, 2014b]. Because only deep convective cloud cases are chosen, the influence caused by cloud regimes is not discussed here. However, the aerosol effect on precipitation and CAPE might differ depending on environmental parameters. The 500 mb VV, 2 m level RH, and 2 m level AT variables were extracted from the CFSR data set. Histograms of each variable were made, and the median values were determined. These median values of environmental variables were used to sort all rainfall amounts and AOD data into subsets of data associated with high and low values of the environmental variable in question (solid and dashed lines in Figure 7, respectively). Each “high” and “low” subset of data has the same number of samples.

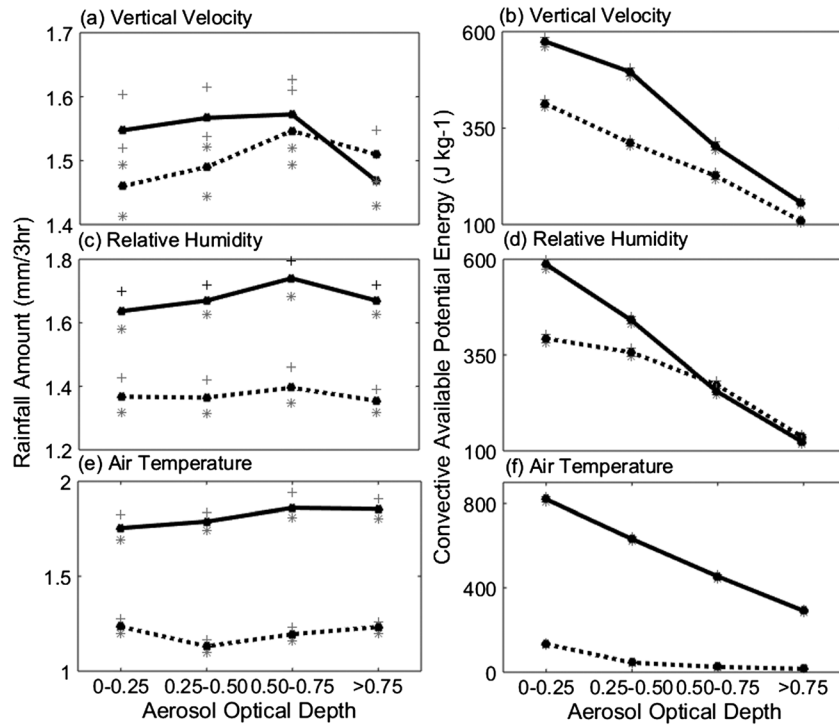


**Figure 7.** (a, c, and e) Mean rainfall amount and (b, d, and f) convective available potential energy as a function of aerosol optical depth range for different conditions: in Figures 7a and 7b, upward vertical velocity (VV), solid lines represent  $VV < -0.035 \text{ Pa s}^{-1}$  and dashed lines represent  $VV > -0.035 \text{ Pa s}^{-1}$ ; in Figures 7c and 7d, relative humidity (RH), solid lines represent  $RH > 89.5\%$  and dashed lines represent  $RH < 89.5\%$ ; in Figures 7e and 7f, 2 m level air temperature (AT), solid lines represent  $AT > 292 \text{ K}$  and dashed lines represent  $AT < 292 \text{ K}$ . The plus and asterisk marks show the bootstrap confidence interval of the mean at the 95% confidence interval.

The rainfall amount and CAPE characteristics discussed previously are plotted in Figure 7. It is clear that CAPE values are larger under high upward vertical velocity, high relative humidity, and warmer temperature conditions (Figures 7b, 7d, and 7f). This is not surprising because higher values of CAPE are typically associated with stronger, more vertically developed clouds [Storer *et al.*, 2014] and greater moisture and heating conditions. The statistically significant decreasing trend in CAPE as AOD increases is seen in all situations, which suggests that the influence of aerosols on the energy redistribution in the atmosphere is independent under different meteorological conditions. However, the trends in rainfall amount with AOD are dependent on the environment. The up-and-down trends for rainfall amount are generally seen for larger 500 mb VV, 2 m level RH, and 2 m level AT values (solid lines in Figures 7a, 7c, and 7e). The up-and-down trend in rainfall amount with AOD is only statistically significant under high RH conditions (Figure 7c). RH not only leads to changes in rainfall amount but also has an influence on the sign of the precipitation response to aerosols. Previous research by Khain *et al.* [2008] also demonstrated the important role of RH in determining the precipitation response to the aerosol signal. Regarding the trend in rainfall amount with AOD under different VV and AT conditions, the signal of the trend is not significant so that it is difficult to detect information confidently here. Note that the response of precipitation to aerosols may also be influenced by meteorological covariations [Gryspeerd *et al.*, 2014a] that are hard to remove in this study.

#### 4. Summary and Discussion

The probabilities of precipitation from different cloud types are calculated using ISCCP cloud data and gauge-based precipitation data from China. Deep convective clouds in eastern China, where aerosol loading is particularly high, are chosen to study the impact of aerosols on precipitation. Downwelling shortwave radiation at the surface, ground heat fluxes, CAPE from the CFSR data set, and AOD at 550 nm from the MERRAero reanalysis are used to examine the effects of aerosols.

The relationship between rainfall amounts from deep convective clouds and aerosol loading follows an up-and-down trend as aerosol loading increases. Before and beyond the critical AOD value, cloud development is enhanced and weakened with rainfall amounts increasing and decreasing in response to increasing AOD. They are likely the signs of the combination of aerosol-radiation interaction (ARI) and aerosol-cloud interaction (ACI).

The ACI and ARI could explain the ascending and descending trends of rainfall changes with increasing AOD. The ascending part of the trend in rainfall amounts from deep convective clouds is likely caused by the aerosol invigoration effect (AIV) originated from the ACI, although the invigoration may also be explained by the changes in cold pool settings due to aerosol-induced enhancement of cloud droplet evaporation, which changes convection in such a way that it becomes optimal for cloud invigoration. The descending part of the trend may be explained by the suppression of solar radiative flux, the ground fluxes, and CAPE that is shown to decrease with increasing AOD.

The impact of aerosols on precipitation may vary depending on different environmental conditions [Storer *et al.*, 2014; Wall *et al.*, 2014]. To help understand the environmental impact, rainfall amounts and CAPE were also analyzed as a function of AOD under different meteorological conditions (vertical velocity, relative humidity, and air temperature). The notable decreasing trends of CAPE with increasing AOD are found to be independent of environmental conditions, while the up-and-down trend in rainfall amount with increasing AOD is only statistically significant under high relative humidity condition, which is consistent with the results from Khain *et al.* [2008], although meteorological covariations [Gryspeerd *et al.*, 2014a, 2014b] cannot be ruled out. While the reduction in CAPE is consistent with the ARI-induced decrease in CAPE, CAPE used in this study is calculated using environmental profiles that do not consider the invigoration caused by extra latent heat release from freezing.

#### Acknowledgments

This study was supported by the Ministry of Science and Technology of China (2013CB955804), State Key Laboratory of Earth Surface Processes and Resource Ecology (2015-TDZD-090), the National Science Foundation (1534670), and NOAA (NA15NWS4680011). We would like to thank the Chinese Meteorological Administration's National Meteorological Information Center, (<http://cdc.cma.cn> and <http://data.cma.cn/>), the NASA Goddard Space Flight Center (<http://gmao.gsfc.nasa.gov/research/merra/>), the International Satellite Cloud Climatology Project (<http://isccp.giss.nasa.gov/products/onlineData.html> and <ftp://eclipse.ncdc.noaa.gov/san1/isccp/dx/>), and the Computational Information Systems Laboratory Research Data Archive (<http://rda.ucar.edu/pub/cfsr.html>) for the various data sets employed in this study. We would also like to thank Xiquan Dong, Yi Deng, Jiwen Fan, Qiang Fu, Jianping Guo, Pat Kablick, Seoung-Soo Lee, Jianjun Liu, Timothy Logan, Manoj G. Manguttathil, Mian Qin, Daniel Rosenfeld, Yan Shen, Arlindo da Silva, Kaicun Wang, Anyuan Xiong, Chuanfeng Zhao, and Yuejian Zhu (in alphabetical order of the last name) for their helpful advice regarding this study. We also greatly appreciate the valuable comments from the anonymous reviewers.

#### References

- Ackerman, A. S., O. B. Toon, D. E. Stevens, A. J. Heymsfield, V. Ramanathan, and E. J. Welton (2000), Reduction of tropical cloudiness by soot, *Science*, *288*(5468), 1042–1047, doi:10.1126/science.288.5468.1042.
- Ackerman, T. P. (1977), A model of the effect of aerosols on urban climates with particular applications to the Los Angeles basin, *J. Atmos. Sci.*, *34*(3), 531–547, doi:10.1175/1520-0469(1977)034<0531:AMOTEO>2.0.CO;2.
- Albrecht, B. A. (1989), Aerosols, cloud microphysics, and fractional cloudiness, *Science*, *245*(4923), 1227–1230, doi:10.1126/science.245.4923.1227.
- Andreae, M. O., D. Rosenfeld, P. Artaxo, A. A. Costa, G. P. Frank, K. M. Longo, and M. A. F. Silva-Dias (2004), Smoking rain clouds over the Amazon, *Science*, *303*(5662), 1337–1342, doi:10.1126/science.1092779.
- Barbaro, E., J. Vilà-Guerau de Arellano, H. G. Ouwersloot, J. S. Schröter, D. P. Donovan, and M. C. Krol (2014), Aerosols in the convective boundary layer: Shortwave radiation effects on the coupled land-atmosphere system, *J. Geophys. Res. Atmos.*, *119*, 5845–5863, doi:10.1002/2013JD021237.
- Buchard, V., A. M. da Silva, P. R. Colarco, A. Darmenov, C. A. Randles, R. Govindaraju, O. Torres, J. Campbell, and R. Spurr (2015), Using the OMI aerosol index and absorption aerosol optical depth to evaluate the NASA MERRA Aerosol Reanalysis, *Atmos. Chem. Phys.*, *15*, 5743–5760, doi:10.5194/acp-15-5743-2015.
- Cheng, C. T., W. C. Wang, and J. P. Chen (2007), A modelling study of aerosol impacts on cloud microphysics and radiative properties, *Q. J. R. Meteorol. Soc.*, *133*(623), 283–297, doi:10.1002/Qj.25.
- Chin, M., P. Ginoux, S. Kinne, O. Torres, B. Holben, B. N. Duncan, R. V. Martin, J. Logan, A. Higurashi, and T. Nakajima (2002), Tropospheric aerosol optical thickness from the GOCART model and comparisons with satellite and Sun photometer measurements, *J. Atmos. Phys.*, *59*, 461–483, doi:10.1175/1520-0469(2002)059<0461:TAOTFT>2.0.CO;2.
- Chin, M., T. Diehl, Q. Tan, J. M. Prospero, R. A. Kahn, L. A. Remer, and X. P. Zhao (2013), Multi-decadal variations of atmospheric aerosols from 1980 to 2009: Sources and regional trends, *Atmos. Chem. Phys. Discuss.*, *13*(7), 19,751–19,835, doi:10.5194/acpd-13-19751-2013.
- da Silva, A., P. R. Colarco, A. S. Darmenov, V. Buchard-Marchant, C. A. Randles, and P. Gupta (2011), An overview of the GEOS-5 Aerosol Reanalysis, Abstract A52D-09 presented at 2011 Fall Meeting, AGU, San Francisco, Calif.
- Dee, D., L. Rukhovets, R. Todling, A. da Silva, and J. Larson (2001), An adaptive buddy check for observational quality control, *Q. J. R. Meteorol. Soc.*, *127*, 2451–2471, doi:10.1002/qj.49712757714.
- Fan, J., L. R. Leung, D. Rosenfeld, Q. Chen, Z. Li, J. Zhang, and H. Yan (2013), Microphysical effects determine macrophysical response for aerosol impacts on deep convective clouds, *Proc. Natl. Acad. Sci. U.S.A.*, *110*(48), E4581–E4590, doi:10.1073/pnas.1316830110.
- Fan, J., D. Rosenfeld, Y. Yang, C. Zhao, L. R. Leung, and Z. Li (2015), Substantial contribution of anthropogenic air pollution to catastrophic floods in Southwest China, *Geophys. Res. Lett.*, *42*, 6066–6075, doi:10.1002/2015GL064479.
- Fan, J. W., T. L. Yuan, J. M. Comstock, S. Ghan, A. Khain, L. R. Leung, Z. Q. Li, V. J. Martins, and M. Ovchinnikov (2009), Dominant role by vertical wind shear in regulating aerosol effects on deep convective clouds, *J. Geophys. Res.*, *114*, D22206, doi:10.1029/2009JD012352.
- Feingold, G. (2003), First measurements of the Twomey indirect effect using ground-based remote sensors, *Geophys. Res. Lett.*, *30*(6), 1287, doi:10.1029/2002GL016633.
- Gandin, L. S. (1965), *Objective Analysis of Meteorological Fields*, pp. 242, Isr. Program for Sci. Transl., Jerusalem.
- Grant, L. D., and S. C. van den Heever (2014), Aerosol-cloud-land surface interactions within tropical sea breeze convection, *J. Geophys. Res. Atmos.*, *119*, 8340–8361, doi:10.1002/2014JD021912.
- Grant, L. D., and S. C. van den Heever (2015), Cold pool and precipitation responses to aerosol loading: modulation by dry layers, *J. Atmos. Sci.*, *72*(4), 1398–1408, doi:10.1175/JAS-D-14-0260.1.

- Gryspeerd, E., P. Stier, and D. G. Partridge (2014a), Satellite observations of cloud regime development: The role of aerosol processes, *Atmos. Chem. Phys.*, *14*(3), 1141–1158, doi:10.5194/acp-14-1141-2014.
- Gryspeerd, E., P. Stier, and D. G. Partridge (2014b), Links between satellite-retrieved aerosol and precipitation, *Atmos. Chem. Phys.*, *14*(18), 9677–9694, doi:10.5194/acp-14-9677-2014.
- Guo, J., M. Deng, S. S. Lee, F. Wang, Z. Li, P. Zhai, H. Liu, W. Lv, W. Yao, and X. Li (2016), Delaying precipitation and lightning by air pollution over the Pearl River Delta. Part I: Observational analyses, *J. Geophys. Res. Atmos.*, *121*, 6472–6488, doi:10.1002/2015JD023257.
- Hahn, C. J., W. B. Rossow, and S. G. Warren (2001), ISCCP cloud properties associated with standard cloud types identified in individual surface observations, *J. Clim.*, *14*(1), 11–28, doi:10.1175/1520-0442(2001)014<0011:ICPAWS>2.0.CO;2.
- Hesterberg, T., D. S. Moore, S. Monaghan, A. Clipson, and R. Epstein (2006), Bootstrap methods and permutation tests, in *Introduction to the Practice of Statistics*, 5th ed., edited by D. S. Moore, and G. P. McCabe, chap. 14, pp. 14-1–14-70, W. H. Freeman, New York.
- Intergovernmental Panel on Climate Change (2013), Climate Change 2013: The Physical Science Basis, in *Contribution of Working Group I to the Fifth Assessment Report of the Intergovernmental Panel on Climate Change*, Cambridge Univ. Press, Cambridge, U. K.
- Jiang, H. L., H. W. Xue, A. Teller, G. Feingold, and Z. Levin (2006), Aerosol effects on the lifetime of shallow cumulus, *Geophys. Res. Lett.*, *33*, L14806, doi:10.1029/2006GL026024.
- Kaufman, Y. J., and R. S. Fraser (1997), The effect of smoke particles on clouds and climate forcing, *Science*, *277*(5332), 1636–1639, doi:10.1126/science.277.5332.1636.
- Khain, A., N. BenMoshe, and A. Pokrovsky (2008), Factors determining the impact of aerosols on surface precipitation from clouds: An attempt at classification, *J. Atmos. Sci.*, *65*(5), 1721–1748, doi:10.1175/2007JAS2515.1.
- Kishcha, P., A. M. da Silva, B. Starobinets, and P. Alpert (2014), Air pollution over the Ganges basin and northwest Bay of Bengal in the early postmonsoon season based on NASA MERRAero data, *J. Geophys. Res. Atmos.*, *119*, 1555–1570, doi:10.1002/2013JD020328.
- Koren, I., Y. J. Kaufman, D. Rosenfeld, L. A. Remer, and Y. Rudich (2005), Aerosol invigoration and restructuring of Atlantic convective clouds, *Geophys. Res. Lett.*, *32*, L14828, doi:10.1029/2005GL023187.
- Koren, I., J. V. Martins, L. A. Remer, and H. Afang (2008), Smoke invigoration versus inhibition of clouds over the Amazon, *Science*, *321*(5891), 946–949, doi:10.1126/science.1159185.
- Koren, I., G. Feingold, and L. A. Remer (2010), The invigoration of deep convective clouds over the Atlantic: Aerosol effect, meteorology or retrieval artifact?, *Atmos. Chem. Phys.*, *10*(18), 8855–8872, doi:10.5194/acp-10-8855-2010.
- Koren, I., G. Dagan, and O. Altaratz (2014), From aerosol-limited to invigoration of warm convective clouds, *Science*, *344*(6188), 1143–1146, doi:10.1126/science.1252595.
- Lebo, Z. J. (2014), The sensitivity of a numerically simulated idealized squall line to the vertical distribution of aerosols, *J. Atmos. Sci.*, *71*(12), 4581–4596, doi:10.1175/JAS-D-14-0068.1.
- Lebo, Z. J., and H. Morrison (2014), Dynamical effects of aerosol perturbations on simulated idealized squall lines, *Mon. Weather Rev.*, *142*(3), 991–1009, doi:10.1175/MWR-D-13-00156.1.
- Lee, K. H., Z. Li, M. C. Cribb, J. Liu, L. Wang, Y. Zheng, X. Xia, H. Chen, and B. Li (2010), Aerosol optical depth measurements in eastern China and a new calibration method, *J. Geophys. Res.*, *115*, D00K11, doi:10.1029/2009JD012812.
- Li, G. H., Y. Wang, and R. Y. Zhang (2008), Implementation of a two-moment bulk microphysics scheme to the WRF model to investigate aerosol-cloud interaction, *J. Geophys. Res.*, *113*, D15211, doi:10.1029/2007JD009361.
- Li, Z., et al. (2007), Preface to special section on East Asian Studies of Tropospheric Aerosols: An International Regional Experiment (EAST-AIRE), *J. Geophys. Res.*, *112*, D22S00, doi:10.1029/2007JD008853.
- Li, Z., K. H. Lee, Y. Wang, J. Xin, and W. M. Hao (2010), First observation-based estimates of cloud-free aerosol radiative forcing across China, *J. Geophys. Res.*, *115*, D00K18, doi:10.1029/2009JD013306.
- Li, Z., F. Niu, J. Fan, Y. Liu, D. Rosenfeld, and Y. Ding (2011a), Long-term impacts of aerosols on the vertical development of clouds and precipitation, *Nat. Geosci.*, *4*(12), 888–894, doi:10.1038/ngeo1313.
- Li, Z., et al. (2011b), East Asian Studies of Tropospheric Aerosols and their Impact on Regional Climate (EAST-AIRC): An overview, *J. Geophys. Res.*, *116*, D00K34, doi:10.1029/2010JD015257.
- Lin, J. C., T. Matsui, R. A. Pielke, and C. Kummerow (2006), Effects of biomass-burning-derived aerosols on precipitation and clouds in the Amazon Basin: A satellite-based empirical study, *J. Geophys. Res.*, *111*, D19204, doi:10.1029/2005JD006884.
- Niu, F., and Z. Li (2012), Systematic variations of cloud top temperature and precipitation rate with aerosols over the global tropics, *Atmos. Chem. Phys.*, *12*(18), 8491–8498, doi:10.5194/acp-12-8491-2012.
- Nowottnick, E. P., P. R. Colarco, E. J. Welton, and A. da Silva (2015), Use of the CALIOP vertical feature mask for evaluating global aerosol models, *Atmos. Meas. Tech.*, *8*, 3647–3669, doi:10.5194/amt-8-3647-2015.
- Peng, J., Z. Li, H. Zhang, J. Liu, and M. C. Cribb (2016), Systematic changes in cloud radiative forcing with aerosol loading for deep clouds in the tropics, *J. Atmos. Sci.*, *73*, 231–249, doi:10.1175/JAS-D-15-0080.1.
- Rienecker, M. M., et al. (2008), The GEOS-5 Data Assimilation System Documentation of Versions 5.0. 1, 5.1. 0, and 5.2. 0, *NASA/TM-2008-104606*, vol. 27, 118 pp., NASA Goddard Space Flight Cent., Greenbelt, Md.
- Rienecker, M. M., et al. (2011), MERRA: NASA's Modern-Era Retrospective Analysis for Research and Applications, *J. Clim.*, *24*(14), 3624–3648, doi:10.1175/JCLI-D-11-00015.1.
- Rosenfeld, D. (1999), TRMM observed first direct evidence of smoke from forest fires inhibiting rainfall, *Geophys. Res. Lett.*, *26*(20), 3105–3108, doi:10.1029/1999GL006066.
- Rosenfeld, D. (2000), Suppression of rain and snow by urban and industrial air pollution, *Science*, *287*(5459), 1793–1796, doi:10.1126/science.287.5459.1793.
- Rosenfeld, D., and I. M. Lensky (1998), Satellite-based insights into precipitation formation processes in continental and maritime convective clouds, *Bull. Am. Meteorol. Soc.*, *79*(11), 2457–2476, doi:10.1175/1520-0477(1998)079<2457:SBIIPF>2.0.CO;2.
- Rosenfeld, D., U. Lohmann, G. B. Raga, C. D. O. Dowd, M. Kulmala, S. Fuzzi, A. Reissell, and M. O. Andreae (2008), Flood or drought: How do aerosols affect precipitation?, *Science*, *321*(5894), 1309–1313, doi:10.1126/science.1160606.
- Rossow, W. B., and L. C. Garder (1993), Validation of ISCCP cloud detections, *J. Clim.*, *6*(12), 2370–2393, doi:10.1175/1520-0442(1993)006<2370:VOICD>2.0.CO;2.
- Rossow, W. B., and R. A. Schiffer (1999), Advances in understanding clouds from ISCCP, *Bull. Am. Meteorol. Soc.*, *80*(11), 2261–2287, doi:10.1175/1520-0477(1999)080<2261:AIUCFI>2.0.CO;2.
- Rossow, W. B., A. W. Walker, and L. C. Garder (1993), Comparison of ISCCP and other cloud amounts, *J. Clim.*, *6*(12), 2394–2418, doi:10.1175/1520-0442(1993)006<2394:COIAOC>2.0.CO;2.
- Saha, S., et al. (2010), The NCEP climate forecast system reanalysis, *Bull. Am. Meteorol. Soc.*, *91*(8), 1015–1057, doi:10.1175/2010BAMS3001.1.

- Schiffer, R. A., and W. B. Rossow (1983), The International Satellite Cloud Climatology Project (ISCCP)—The first project of the World Climate Research Programme, *Bull. Am. Meteorol. Soc.*, *64*(7), 779–784.
- Shen, Y., A. Xiong, Y. Wang, and P. Xie (2010), Performance of high-resolution satellite precipitation products over China, *J. Geophys. Res.*, *115*, D02114, doi:10.1029/2009JD012097.
- Storer, R. L., and S. C. van den Heever (2013), Microphysical processes evident in aerosol forcing of tropical deep convective clouds, *J. Atmos. Sci.*, *70*(2), 430–446, doi:10.1175/JAS-D-12-076.1.
- Storer, R. L., S. C. van den Heever, and T. S. L'Ecuyer (2014), Observations of aerosol-induced convective invigoration in the tropical east Atlantic, *J. Geophys. Res. Atmos.*, *119*, 3963–3975, doi:10.1002/2013JD020272.
- Tao, W. K., X. Li, A. Khain, T. Matsui, S. Lang, and J. Simpson (2007), Role of atmospheric aerosol concentration on deep convective precipitation: Cloud-resolving model simulations, *J. Geophys. Res.*, *112*, D24S18, doi:10.1029/2007JD008728.
- Tao, W. K., J. P. Chen, Z. Li, C. Wang, and C. Zhang (2012), Impact of aerosols on convective clouds and precipitation, *Rev. Geophys.*, *50*, RG2001, doi:10.1029/2011RG000369.
- Twomey, S. A., M. Piepgrass, and T. L. Wolfe (1984), An assessment of the impact of pollution on global cloud albedo, *Tellus B*, *36*(5), 356–366, doi:10.1111/j.1600-0889.1984.tb00254.x.
- van den Heever, S. C., and W. R. Cotton (2007), Urban aerosol impacts on downwind convective storms, *J. Appl. Meteorol. Climatol.*, *46*(6), 828–850, doi:10.1175/Jam2492.1.
- Wall, C., E. Zipsper, and C. Liu (2014), An investigation of the aerosol indirect effect on convective intensity using satellite observations, *J. Atmos. Sci.*, *71*(1), 430–447, doi:10.1175/JAS-D-13-0158.1.
- Wang, C. (2005), A modeling study of the response of tropical deep convection to the increase of cloud condensation nuclei concentration: Dynamics and microphysics, *J. Geophys. Res.*, *110*, D21211, doi:10.1029/2004JD005720.
- Wang, Y., Q. Wan, W. Meng, F. Liao, H. Tan, and R. Zhang (2011), Long-term impacts of aerosols on precipitation and lightning over the Pearl River Delta megacity area in China, *Atmos. Chem. Phys.*, *11*, 12,421–12,436, doi:10.5194/acp-11-12421-2011.
- Wei, L., Q. Zhong, and P. Hou (1996), Evaluation on cloud variables from ISCCP data over Chinese continent [in Chinese], *Plateau Meteorol.*, *15*(2), 147–156.
- Weng, D., and A. Han (1998), Comparison analysis of total cloud amount in satellite and ground-based in China [in Chinese], *J. Appl. Meteorol. Sci.*, *9*(1), 32–37.
- Wu, G., et al. (2016), Advances in studying interactions between aerosols and monsoon in China, *Sci. China*, *59*, 1–16, doi:10.1007/s11430-015-5198-z.
- Xie, P. P., A. Yatagai, M. Y. Chen, T. Hayasaka, Y. Fukushima, C. M. Liu, and S. Yang (2007), A gauge-based analysis of daily precipitation over East Asia, *J. Hydrometeorol.*, *8*(3), 607–626, doi:10.1175/Jhm583.1.
- Xin, J., et al. (2007), Aerosol optical depth (AOD) and Angstrom exponent of aerosols observed by the Chinese Sun Hazemeter Network from August 2004 to September 2005, *J. Geophys. Res.*, *112*, D05203, doi:10.1029/2006JD007075.
- Yan, H., Z. Li, J. Huang, M. C. Cribb, and J. Liu (2014), Long-term aerosol-mediated changes in cloud radiative forcing of deep clouds at the top and bottom of the atmosphere over the Southern Great Plains, *Atmos. Chem. Phys.*, *14*(14), doi:10.5194/acp-14-7113-2014.
- Yuan, T., Z. Li, R. Zhang, and J. Fan (2008), Increase of cloud droplet size with aerosol optical depth: An observation and modeling study, *J. Geophys. Res.*, *113*, D04201, doi:10.1029/2007JD008632.
- Zhang, Y., and X. W. Li (1992), *Office of China Flood Prevention and Drought Resistance Headquarter, Flood Prevention Manual* [in Chinese], China Science and Technology Press, Beijing.